Demixing in the Low Power Argon/Helium Arcjet

IEPC-2013-369

*Presented at the 33rd International Electric Propulsion Conference,
The George Washington University • Washington, D.C. • USA
October 6 – 10, 2013*

Jinyue Geng[1], Xuan Chen[2] and Hai-Xing Wang[3]
Beijing University of Aeronautics and Astronautics, Beijing, 100191, China

and

Michael Keidar[4]
George Washington University, Washington DC 20052, USA

Abstract: A modeling study is performed to investigate the demixing process in the low power arcjet. The all-speed SIMPLE algorithm is employed to solve the governing equations, which takes into account the effects of compressibility, Joule heating and the Lorentz force, as well as the temperature, pressure and component dependence of the gas properties. Demixing is treated by introducing a conservation equation for one of the gases and making use of the combined diffusion coefficient method. The modeling results show that considering demixing leads to a larger heat flux to the anode, but no significant effects on the flow characteristics in the nozzle.

Nomenclature

c_p	=	specific heat at constant pressure
$\overline{D}_{AB}^{P}$	=	combined pressure diffusion coefficient
$\overline{D}_{AB}^{T}$	=	combined temperature diffusion coefficient
$\overline{D}_{AB}^{x}$	=	combined ordinary diffusion coefficient
e	=	elementary charge
h	=	specific enthalpy
k_B	=	Boltzmann constant
$\overline{m}_A$	=	average mass of heavy species of gas A
$\overline{m}_B$	=	average mass of heavy species of gas B
n	=	plasma number density
p	=	gas pressure
T	=	temperature
U_r	=	radiation power per unit volume of plasma
u	=	axial (z-) component of the velocity vector $\boldsymbol{V}$
v	=	radial (r-) component of the velocity vector $\boldsymbol{V}$
$\overline{X}_A$	=	mole fraction of all the components of gas A

[1] PhD Student, School of Astronautics, gengjinyue@sa.buaa.edu.cn.
[2] Graduate Student, School of Astronautics, chenxuan@sa.buaa.edu.cn.
[3] Professor, School of Astronautics, whx@buaa.edu.cn.
[4] Professor, Department of Mechanical and Aerospace Engineering, keidar@gwu.edu.

ϕ	=	electric potential
ρ	=	gas density
μ	=	viscosity
κ	=	thermal conductivity
σ	=	electrical conductivity

I. Introduction

DURING the past several decades, electric propulsion research has been largely commercialized for stationkeeping, and orbit topping applications[1]. The arcjet thrusters can be operated by a variety of different propellants such as hydrogen, argon, helium, nitrogen, ammonia etc. In most of ground-based tests, the mixtures of two different gases are often used as working gas to investigate the performance of arcjet thruster. In the previous simulation studies, the assumption usually used is that the mixture gases remain fully mixed. But it has been found that demixing due to diffusion, which driven by the temperature gradients and pressure gradients, can lead to the partial separation of gases in arcs, particularly when the gases have very different masses, such as in argon–helium and argon–hydrogen arcs[2, 3]. Normally, the partial separation of gases in arcs will affect the gas properties, and the affects the performances of the thruster. Modeling studies are conducted for the low-power (kW class) arcjet thruster[4] designed by NASA Lewis Research Center.

II. Modeling Approach

The main assumptions employed in the modeling study are as follows. (i) the gas flow in the arcjet nozzle is steady, axisymmetric, laminar and compressible; (ii) the bulk plasma is in the LTE (local thermodynamic equilibrium) state and thus the thermodynamic and transport properties of argon/helium mixtures are completely determined by the gas temperature pressure and component; non-LTE effects are only considered by appropriately increasing the values of gas electrical conductivity in the near-anode region, as suggested in [4, 5]; (iii) the plasma is optically thin to radiation; (iv) the azimuthal (swirling) velocity component is negligible in comparison with the axial velocity component, and (v) the flow-induced electric field is negligible in comparison with the static electric field. Based on these assumptions, the governing equations in the cylindrical coordinate system can be written as follows[4, 6]:

$$\frac{\partial}{\partial z}(\rho u) + \frac{1}{r}\frac{\partial}{\partial r}(r\rho v) = 0 \tag{1}$$

$$\frac{\partial(\rho uu)}{\partial z} + \frac{1}{r}\frac{\partial(r\rho uv)}{\partial r} = -\frac{\partial p}{\partial z} + 2\frac{\partial}{\partial z}\left(\mu\frac{\partial u}{\partial z}\right) + \frac{1}{r}\frac{\partial}{\partial r}\left[r\mu\left(\frac{\partial u}{\partial r} + \frac{\partial v}{\partial z}\right)\right] + j_r B_\theta \tag{2}$$

$$\frac{\partial(\rho uv)}{\partial z} + \frac{1}{r}\frac{\partial(r\rho vv)}{\partial r} = -\frac{\partial p}{\partial r} + \frac{2}{r}\frac{\partial}{\partial r}\left(r\mu\frac{\partial v}{\partial r}\right) + \frac{\partial}{\partial z}\left[\mu\left(\frac{\partial v}{\partial z} + \frac{\partial u}{\partial r}\right)\right] - 2\mu\frac{v}{r^2} - j_z B_\theta \tag{3}$$

$$\begin{aligned}\frac{\partial(\rho uh)}{\partial z} + \frac{1}{r}\frac{\partial(r\rho vh)}{\partial r} = {} & \frac{\partial}{\partial z}\left[\frac{k}{c_p}\frac{\partial h}{\partial z}\right] + \frac{1}{r}\frac{\partial}{\partial r}\left[r\frac{k}{c_p}\frac{\partial h}{\partial r}\right] + u\frac{\partial p}{\partial z} + v\frac{\partial p}{\partial r} + \Phi + \frac{j_z^2 + j_r^2}{\sigma} + \frac{5k_B}{2e}\left(\frac{j_z}{c_P}\frac{\partial h}{\partial z} + \frac{j_r}{c_P}\frac{\partial h}{\partial r}\right) \\ & - \frac{2}{3}\mu(\nabla\cdot\vec{V})^2 - U_r - \frac{\partial}{\partial z}\left[(h_A - h_B)J_z\right] - \frac{1}{r}\frac{\partial}{\partial r}\left[r(h_A - h_B)J_r\right] - \frac{\partial}{\partial z}\left[\frac{k}{c_p}(h_A - h_B)\frac{\partial f_A}{\partial z}\right] - \frac{1}{r}\frac{\partial}{\partial r}\left[r\frac{k}{c_p}(h_A - h_B)\frac{\partial f_A}{\partial r}\right]\end{aligned} \tag{4}$$

$$\frac{1}{r}\frac{\partial}{\partial r}\left(r\sigma\frac{\partial\phi}{\partial r}\right) + \frac{\partial}{\partial z}\left(\sigma\frac{\partial\phi}{\partial z}\right) = 0 \tag{5}$$

$$\frac{\partial(\rho u f_A)}{\partial z} + \frac{1}{r}\frac{\partial(r\rho v f_A)}{\partial r} = \frac{\partial}{\partial z}\left[\Gamma_f\frac{\partial f_A}{\partial z}\right] + \frac{1}{r}\frac{\partial}{\partial r}\left[r\Gamma_f\frac{\partial f_A}{\partial r}\right] + S_f \tag{6}$$

The symbol S_f in Eq. (6) is calculated by[7]

$$S_f = \frac{\partial}{\partial z}\left(\Gamma_f \frac{f_A}{M}\frac{\partial M}{\partial z}\right) - \frac{\partial}{\partial z}\left(\Gamma_f \frac{f_A}{M_A}\frac{\partial M_A}{\partial z}\right) + \frac{1}{r}\frac{\partial}{\partial r}\left(r\Gamma_f \frac{f_A}{M}\frac{\partial M}{\partial r}\right)$$
$$- \frac{1}{r}\frac{\partial}{\partial r}\left(r\Gamma_f \frac{f_A}{M_A}\frac{\partial M_A}{\partial r}\right) + \frac{\partial}{\partial z}\left(\overline{D}_{AB}^{T}\frac{\partial \ln T}{\partial z}\right) + \frac{1}{r}\frac{\partial}{\partial r}\left(r\overline{D}_{AB}^{T}\frac{\partial \ln T}{\partial r}\right)$$
$$- \frac{\partial}{\partial z}\left(\frac{m_A m_B}{M^2}\rho\overline{D}_{AB}^{P}\frac{\partial \ln p}{\partial z}\right) - \frac{1}{r}\frac{\partial}{\partial r}\left(r\frac{m_A m_B}{M^2}\rho\overline{D}_{AB}^{P}\frac{\partial \ln p}{\partial r}\right) \tag{7}$$

where the diffusion coeffience Γ_f is calculated by

$$\Gamma_f = \frac{m_A m_B}{M M_A}\rho\overline{D}_{AB}^{x} \tag{8}$$

The physical properties ρ, c_p, h, μ, κ, σ and U_r are temperature- pressure- and component-dependent, and are calculated for each spatial point based on local temperature and pressure by using pre-compiled LTE plasma property databases (covering the temperature range 300 K – 30000 K and pressure range 10 Pa – 3×10^5 Pa) for each of the studied plasmas.

The Lorentz force terms have been included in the momentum equations (2) and (3) and the Joule heating rate and the electron-enthalpy transport terms have been included in the energy equation (4) in order to include the effects on the plasma flow and heat transfer of electromagnetic fields related to the DC electric arc discharge. Current density components j_r and j_z appearing in Eqs. (2), (3) and (4) are calculated by using

$$j_r = -\sigma\frac{\partial\phi}{\partial r} \qquad j_z = -\sigma\frac{\partial\phi}{\partial z} \tag{9}$$

while the self-induced magnetic induction intensity B_θ is calculated by using

$$B_\theta = \frac{\mu_0}{r}\int_0^r j_z \xi d\xi \tag{10}$$

where μ_0 is the permeability of free space.

In this study, the temperature distribution along the inner surface of the anode nozzle is determined by the iterative computation process itself in this study, instead of being artificially specified. To this end, the energy equation is solved for the solid region, which is listed as follows:

$$\frac{\partial}{\partial z}\left(\kappa_s\frac{\partial T}{\partial z}\right) + \frac{1}{r}\frac{\partial}{\partial r}\left(r\kappa_s\frac{\partial T}{\partial r}\right) + \frac{j_z^2 + j_r^2}{\sigma_s} + \frac{5k_B}{2e}\left(j_z\frac{\partial T}{\partial z} + j_r\frac{\partial T}{\partial r}\right) = 0 \tag{11}$$

Boundary conditions are similar to that used in Ref. [4]. For the Eq. (6), f_A is set 0.9 at the inlet, extrapolated at the outlet, and f_A is calculated by setting the mass flux to the anode $\bar{J}_A = 0$ at the anode surface.

III. Results and Discussion

A. Combined Diffusion Coefficients

The dimixing effect is considered based on the combined diffusion coefficient method, which was used in Refs. [2,3,7]. The diffusion coefficients method, that describes demixing in terms of gases rather than of species as in previous treatments, is an algebraically simple and physically transparent mathematical description of demixing. The combined diffusion coefficients are defined by an expression for the diffusive mass flux of gas A for a two-species gas:

$$\bar{J}_A = -\left(n^2/\rho\right)\overline{m}_A\overline{m}_B\left(\overline{D}_{AB}^{x}\nabla X_A - \overline{D}_{AB}^{P}\nabla \ln p\right) - \overline{D}_{AB}^{T}\nabla \ln T \tag{12}$$

$\overline{D}_{AB}^{x}$, $\overline{D}_{AB}^{P}$ and $\overline{D}_{AB}^{T}$ are calculated by using the method in Refs. [2, 3].

The one-to-one correspondence between combined diffusion coefficients and demixing processes allows the contribution of each process to be calculated separately, thereby allowing the physical causes of demixing to be examined.

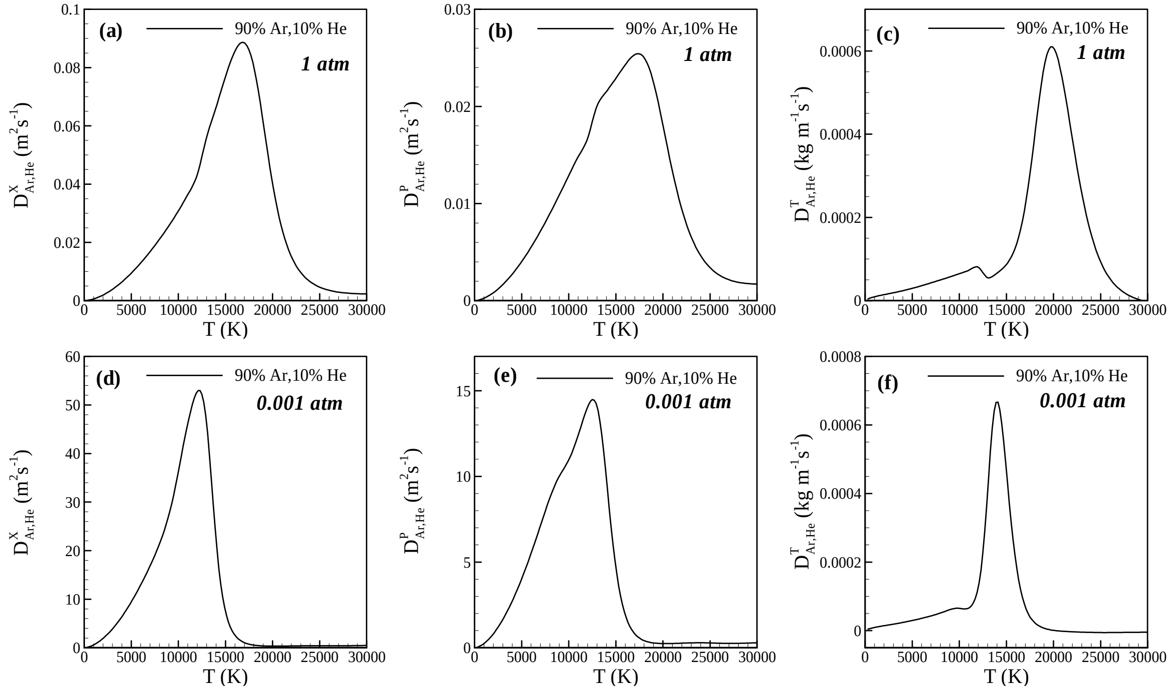

Figure 1. Combined diffusion coefficients for mixture of argon and helium by weight. (a) Combined ordinary diffusion coefficient (*p*=1 atm); (b) combined pressure diffusion coefficient (*p*=1 atm); (c) combined temperature diffusion coefficient (*p*=1 atm); (d) Combined ordinary diffusion coefficient (*p*=0.001 atm); (e) combined pressure diffusion coefficient (*p*=0.001 atm); (f) combined temperature diffusion coefficient (*p*=0.001 atm).

Fig. 1 presents the combined diffusion coefficients at the pressure p=1 atm and p=0.001 atm, which are calculated by A. B. Murphy. It can be concluded that with the decreasing of pressure, the combined ordinary diffusion coefficient and combined pressure diffusion coefficient decrease strongly, but the combined temperature diffusion coefficient has not largely changes.

The Eq. (12) shows the relationship between the mass flux of the gas A (argon) and the gradients of mole fraction, the gradients of pressure and the gradients of temperature. And Fig. 1 shows that the combined diffusion coefficients are all positive, so the following laws can be obtain:

1) The mole fraction gradients drive the argon from the higher mole fraction region to the lower mole fraction region;

2) The pressure gradients drive the argon from the lower pressure region to the higher pressure region;

3) The temperature gradients drive the argon from the higher temperature region to the lower temperature region.

Table I and Table II show the values of the terms $\left(\rho/\overline{M}^2\right)\overline{m}_A\overline{m}_B\overline{D}_{AB}^{P}$ and $\overline{D}_{AB}^{T}$, which are the coefficients of the gradients of pressure and temperature in Eq. (12), near the constrictor and in the near-outlet region of the thruster nozzle. Table I shows that the terms $\left(\rho/\overline{M}^2\right)\overline{m}_A\overline{m}_B\overline{D}_{AB}^{P}$ and $\overline{D}_{AB}^{T}$ have the same order of magnitude. From the constrictor to the outlet of the nozzle, the combined pressure diffusion coefficient $\overline{D}_{AB}^{P}$ largely increases as the pressure decrease to 0.001 atm, but the combined temperature diffusion coefficient $\overline{D}_{AB}^{T}$ keeps the same order of magnitude, which is shown in Fig. 1. But the density decreases and $\overline{M}$ increases as the pressure increases, so the terms $\left(\rho/\overline{M}^2\right)\overline{m}_A\overline{m}_B\overline{D}_{AB}^{P}$ and $\overline{D}_{AB}^{T}$ also have the same order of the magnitude near the outlet, which can be indicate in Table II. So the dominant driven force for demixing depends on the values of gradients of pressure and temperature.

Table I the values of the terms in Eq. (12) near the constrictor (p=1 atm, T=7000 K or 15000 K)

	$\left(\rho/\overline{M}^2\right)\overline{m}_A\overline{m}_B\overline{D}^P_{AB}$	$\overline{D}^T_{AB}$
7000 K	2.64×10^{-5}	4.25×10^{-5}
15000 K	8.7×10^{-5}	8.8×10^{-5}

Table II the values of the terms in Eq. (12) near the outlet (p=0.001 atm, T=3000 K)

	$\left(\rho/\overline{M}^2\right)\overline{m}_A\overline{m}_B\overline{D}^P_{AB}$	$\overline{D}^T_{AB}$
3000 K	1.4×10^{-5}	1.88×10^{-5}

B. Modeling Results and Discussion

In the modeling, the mixture of 90% argon and 10% helium by mass is used as the propellant, the inlet pressure p_{in}=2.5 atm, and the arc current I=10 A. Table III shows the performances of the Arcjet thruster for the case considering demixing and neglect demixing. It can be concluded that the demixing in the argon/helium arcjet leads to larger heat flux to the anode, but due to the small atomic mass of helium (gas B), demixing has no significant effects on the flow characteristics in the nozzle. Accordingly, demixing has no significant effect on the specific impulse and thrust.

Table III the performances of the Arcjet thruster considering demixing and neglect demixing
(Ar:He=9:1 by mass, I=10 A)

	Mass flow rate (mg/s)	The highest velocity (m/s)	The highest temperature (K)	The velocity at the outlet centerline (m/s)	The temperature at the outlet centerline (K)	Thrust (mN)	I_{sp} (s)	The heat flux to anode (W)
Considering demixing	38.1	5280	15978	4672	2085	111.9	300	172.3
Neglect demixing	39.5	5250	15989	4702	2205	119.2	308	132.4

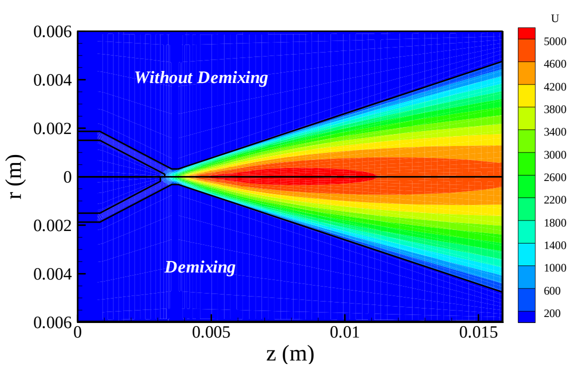

Figure 2. Axial velocity distributions (Unit: m/s).

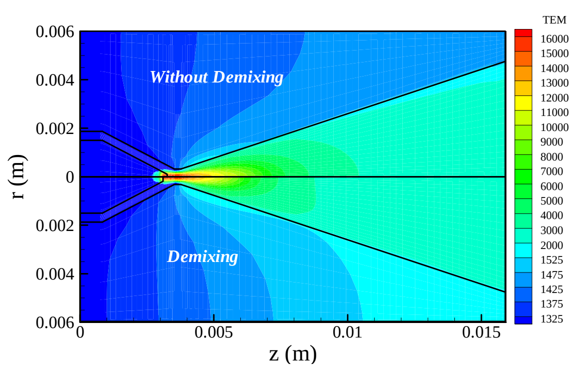

Figure 3. Temperature distributions (Unit: K).

Fig. 2 and 3 compare the computed distributions of axial velocity and gas temperature, respectively, within the thruster nozzle for the case considering demixing and the case neglect demixing. Fig. 2 plots the computed axial velocity distributions in the gas flow region of the nozzle, due to the conversion of the pressure energy and internal energy into the kinetic energy, the gaseous propellant flowing into the nozzle is rapidly accelerated to rather high velocities within a short axial distance. Figure 2 shows that axial velocity distributions within the thruster nozzle are similar overall for the case considering demixing and the case neglect demixing. The computed gas temperature distributions in the gas flow region and in the solid-wall region of the nozzle for the case considering demixing and neglect demixing are shown in Fig.3. It is seen that the considering demixing leads to an increase in the anode temperature.

Fig.4 shows the argon mass fraction distribution in the nozzle when considering demixing. Although the propellant is fully mixed before into the nozzle, the demixing will occur due to the gradients of temperature, pressure and mole fraction, and the argon mass fraction will not be uniform anymore.

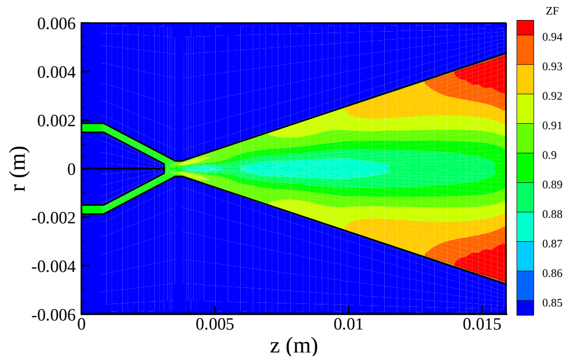

Figure 4. Argon mass fraction.

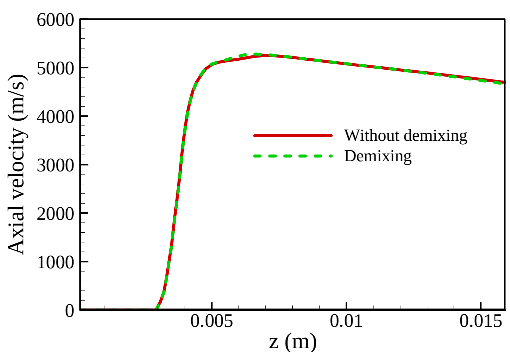

Figure 5. Axial velocity along the axis.

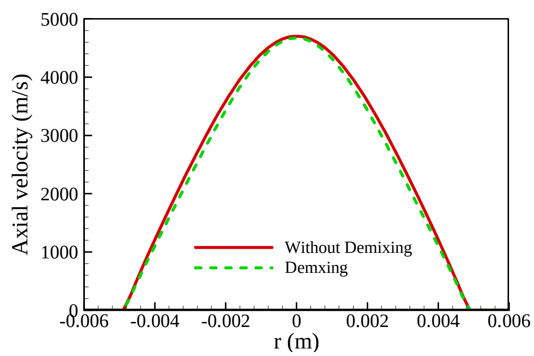

Figure 6. Axial velocity profile at the oulet.

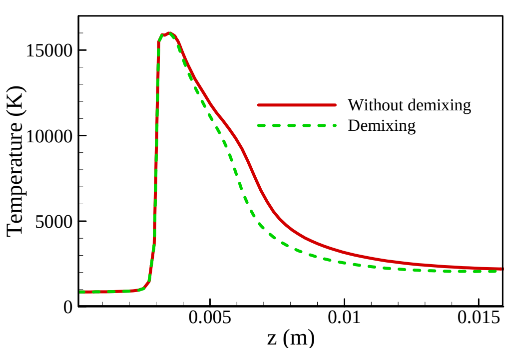

Figure 7. Temperature along the axis.

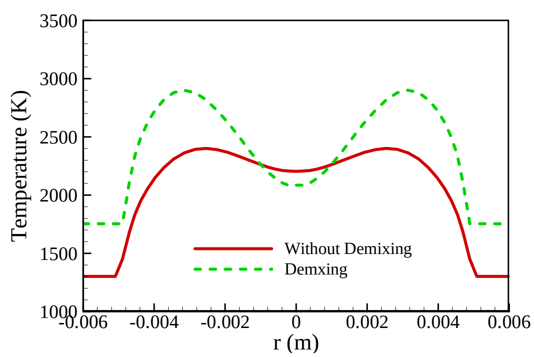

Figure 8. Temperature profile at the oulet.

Fig. 5 and Fig. 6 show the axial velocity along the axis and at the outlet. Fig. 7 and Fig. 8 show the temperature along the axis and at the outlet. The axial velocity has no significant change along the axis and at the oulet plane, but the temperature has large discrepancy. At the outlet plane, the temperature profile considering demixing is more like the non-monotonic temperature profile which has been observed by Walker[8] in an experimental study of a helium arcjet thruster, because of the concentration of helium near the axis.

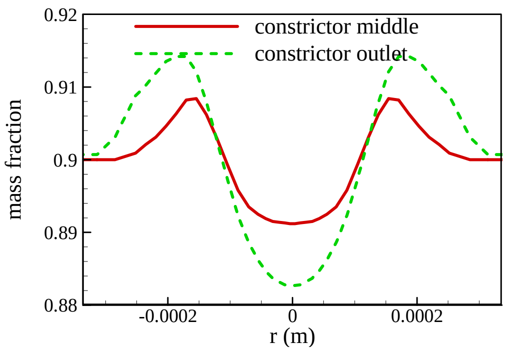

Figure 9. Argon mass fraction profiles in the constrictor.

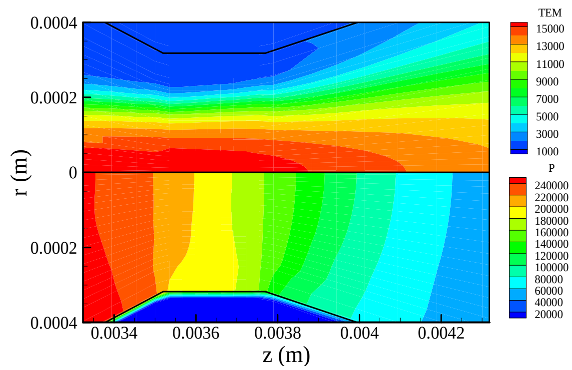

Figure 10. Temperature (K) and pressure (Pa) distributions in the constrictor.

Fig. 9 shows the argon mass fraction radial profiles in the constrictor. From near anode region to axis, the argon mass fraction first increase and then decrease. Fig. 10 shows the temperature and pressure distributions in the constrictor region of the nozzle. There are strongly temperature drops from axis to anode, and largely pressure drops along the axis in the constrictor of the nozzle[4, 9]. Fig. 10 indicates that the pressure is almost constant along the radial direction, so the argon mass fraction radial profiles in the constrictor mostly depend on the temperature distribution.

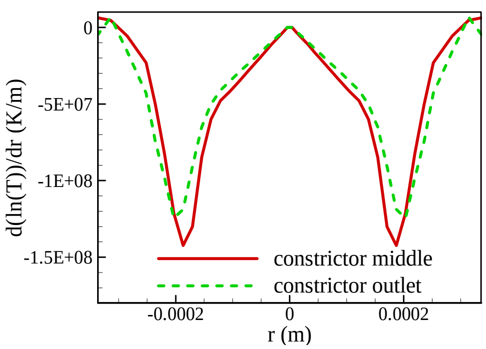

Figure 11. first derivative of *ln*(*T*) with respect to *r*.

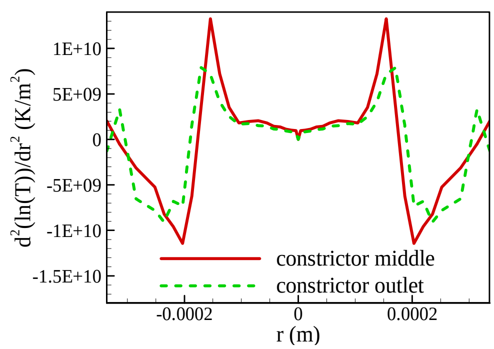

Figure 12. second derivative of *ln*(*T*) with respect to *r*.

Fig. 11 and Fig. 12 show the first derivative and second derivative of *ln*(*T*) with respect to *r*, respectively. It can be concluded from the Eq. (12) that the mass flux of gas A $\vec{J}_A$ is related to $\nabla \ln T$; the Eq. (6) indicates that the argon mass fraction distribution is related to $\nabla \vec{J}_A$. So the argon mass fraction is related to the second derivative of *ln*(*T*) with respect to *r*, the argon mass fraction increases with negative $d^2 \ln T / dr^2$ and decreases with positive $d^2 \ln T / dr^2$. The $d^2 \ln T / dr^2$ is negative first and then changes to positive from anode to axis in Fig. 12, so the argon mass fraction increases first and then decreases from anode to axis, which is shown in Fig. 9.

Fig. 13 and Fig. 14 show the second derivative of *ln*(*P**) and *ln*(*T**) with respect to *z*. Here *P** and *T** are the reduced pressure and temperature, which calculated by Eq. (13).

$$P^* = \frac{\int_0^{r_z} 2\pi r \rho u P dr}{\int_0^{r_z} 2\pi r \rho u dr}, \quad T^* = \frac{\int_0^{r_z} 2\pi r \rho u T dr}{\int_0^{r_z} 2\pi r \rho u dr}. \tag{13}$$

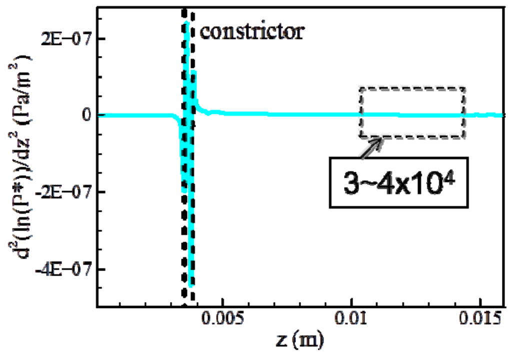

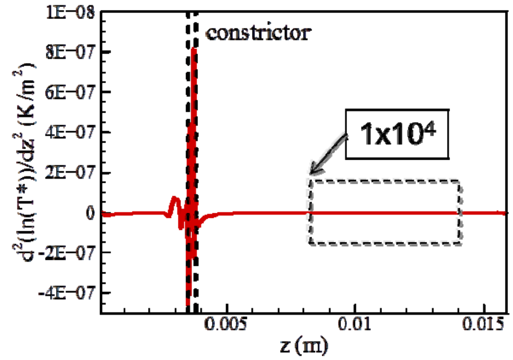

Figure 13. Second derivative of *ln*(*P) with respect to *z*. Figure 14. Second derivative of *ln*(*T**) with respect to *z*.**

The Eq. (6) and Eq. (12) indicate that the argon mass fraction distribution is related to $\nabla\vec{J}_A$, and $\nabla\vec{J}_A$ is related to the second derivative of *ln*(*P*) and *ln*(*T*). The term $\left(\rho/\overline{M}^2\right)\overline{m}_A\overline{m}_B\overline{D}^P_{AB}$ in the Eq. (12) is comparable to $\overline{D}^T_{AB}$, which have been shown in III B, and the second derivative of *ln*(*P**) with respect to *z* is about 3~4 times to the second derivative of *ln*(*T**), so the pressure gradient is the dominant driven force in the divergence region of the nozzle. Because of the positive second derivative of *ln*(*P**), the average argon mass fraction at a cross-section of the divergence region increases along the axis, which can be indicated in Fig. 4.

IV. Conclusion

Numerical simulations have been carried out to study the effect of demixing on the plasma flow and heat transfer of the low-power (kW class) arcjet thruster using the mixture of 90% argon and 10% helium by mass as propellant. Modeling results were compared with the case neglect demixing. The modeling results show that considering demixing leads to an increase in the anode temperature, but no significant change in the axial velocity distribution. This indicates that the demixing in the argon/helium arcjet leads to larger heat flux to the anode, but no significant effects on the flow characteristics in the nozzle. Accordingly, demixing has no significant effect on the specific impulse and thrust. Due to quasi one-dimensional pressure distribution in the constrictor of nozzle, the argon mass fraction is related to second derivative of *ln*(*T*) in the near-constrictor region. And the pressure gradient is the dominant driven force in the divergence region of the nozzle.

Acknowledgments

This work was supported by the National Natural Science Foundation of China (Nos. 11275021, 11072020, 50836007). Authors also gratefully acknowledge the financial support from the China Scholarship Council.

References

[1]Hargus, W. A., et al., “Arcjet plasma neutralization of Hall thrusters, Part 1: Hybrid thruster mission analysis,” *Journal of Spacecraft and Rockets*, Vol. 41, No. 6, 2004, pp. 1016-1022.

[2]Murphy, A. B., “Demixing in free-burning arcs,” *Physical Review E*, Vol. 55, No. 6, 1997, pp. 7473-7494.

[3]Murphy, A. B., “Cataphoresis in electric arcs,” *Journal of Physics D: Applied Physics*, Vol. 31, No. 23, 1998, pp. 3383-3390.

[4]Wang, H. X., et al., “Modeling study on the flow, heat transfer and energy conversion characteristics of low-power arc-heated hydrogen/nitrogen thrusters,” *Plasma Chemistry and Plasma Processing*, Vol. 30, No. 6, 2010, pp. 707-731.

[5]Rhodes, R. P., Keefer, D., “Numerical modeling of an arcjet thruster,” *AIAA 21st International Electric Propulsion Conference*, AIAA No. 90-2614, Orlando, FL, 1990.

[6]Han, P., Chen, X., “Modeling of the subsonic–supersonic flow and heat transfer in a DC arc plasma torch,” P*lasma Chem Plasma Process*, Vol. 21, No. 2, 2001, pp. 249–264.

[7]Murphy, A. B., “Diffusion in equilibrium mixtures of ionized gases,” *Physical Review E*, Vol. 48, No. 5, 1993, pp. 3594-3601.

[8]Walker, Q. E., “Characterization and novel applications of the helium arcjet,” Ph.D. Dissertation, Aeronautics and Astronautics Dept., Stanford Univ., Stanford, CA, 2007.

[9]Wang, H. X., et al., “Numerical investigation of the plasma flow through the constrictor of arc-heated thrusters,” *Journal of Physics D: Applied Physics*, Vol. 45, No. 23, 2012, pp.5202-5213.